

InN dielectric function from the midinfrared to the visible range

L.A. Falkovsky^{1,2}

¹*L.D. Landau Institute for Theoretical Physics, Moscow 117334, Russia*

²*Institute of the High Pressure Physics, Troitsk 142190, Russia*

(Dated: November 15, 2018)

The dispersion of the dielectric function for wurtzite InN is analytically evaluated in the region near the fundamental energy gap. The real part of the dielectric function has a logarithmic singularity at the absorption edge. This results in the large contribution into the optical dielectric constant. For samples with degenerate carriers, the real part of the dielectric function is divergent at the absorption edge. The divergence is smeared with temperatures or relaxation rate. The imaginary part of the dielectric function has a plateau far away from the absorption onset.

PACS numbers: 71.15.Mb, 71.20.Nr, 78.20.Ci

Recently, InN has attracted considerable attention due to its potential application as other III-nitrides, but especially owing to the small energy band gap $2\varepsilon_g$ of about 0.7 eV observed [1, 2, 3, 4, 5] in contrast to the value of 1.9 eV established for the last 20 years. The small band gap value corresponds with a small effective electron mass $m^* \approx 0,07m_0$ [6, 7, 8].

For future progress in the research field, reliable material parameters are derived from the most widespread *ab initio* electronic-structure calculations. However, these methods do not present analytical results and lead sometimes to contradictions [9], whether the 4d bands are included in the core or are not. Therefore, the $\mathbf{k} \cdot \mathbf{p}$ Hamiltonian is used to clarify the physical content. In the corresponding Kane model [10] for the wurtzite case, the conduction-band and the valence-band are constructed from the $|s\rangle$ and $|x\rangle, |y\rangle, |z\rangle$ states at the Γ -point.

In Fig. 1a, the scheme of the valence-band splitting in InN is shown under the crystal field Δ_{CR} and the spin-orbit interaction Δ_{SO} . According to experimental data [11] and calculations [8], this splitting has a value on the order of $0.02 \div 0.06$ eV, i. e. it is small in comparison with the band gap, and can be ignored in calculations of the integral properties as the optical absorption. Therefore, the Kane model can be substantially simplified while using in calculations of the dielectric function (DF).

In this paper with the help of the simplified Kane model, we evaluate analytically the DF for wurtzite InN in the range $\omega \sim 0.3 \div 4$ eV, where the absorption is dominated by optical transitions from three highest valence bands into the lowest conduction band. As well known, the imaginary part of the DF has the square-root behavior near the absorption edge in the case, if the conduction-band is empty (i), and the step-like behavior in the case, if the carriers in the conduction band are degenerate (ii). In the paper [12], the *ab initio* calculations of the imaginary part were presented for the InN polymorphs (with wurtzite, zinc-blend, and rocksalt structures) in the case (i), whereas the real part was restored using the Kramers-Kronig relations. In the paper [12], the imaginary part was also estimated within the Kane model, but these results are misleading, because the optical-transition matrix elements are incorrectly evalu-

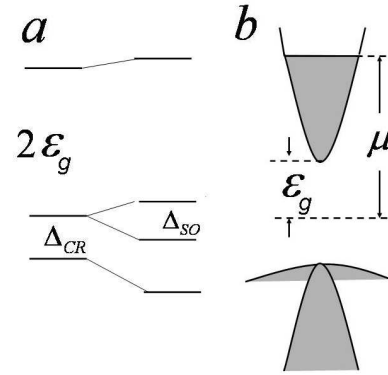


FIG. 1: (a) scheme of the valence-band splitting under the crystal field and the SO interactions; (b) the electron band, the heavy-hole and light-hole bands near the Γ -point.

ated.

We find, that the real part of the DF has at the absorption edge the kink-like singularity in the case (i) and the logarithmic divergence in the case (ii). Such singularities have been previously obtained for graphene [13] and for IV-VI semiconductors [14]. The singularities are smeared with temperatures or carrier relaxation. The excitonic effects was not observed in InN, since they are suppressed by the carrier relaxation (see [6, 12, 15] for their estimation).

The effective Hamiltonian of the simplified anisotropic Kane model is given as the matrix 4×4 :

$$H = \begin{pmatrix} \varepsilon_g & iP_2k_x & iP_2k_y & iP_1k_z \\ -iP_2k_x & -\varepsilon_g & 0 & 0 \\ -iP_2k_y & 0 & -\varepsilon_g & 0 \\ -iP_1k_z & 0 & 0 & -\varepsilon_g \end{pmatrix}, \quad (1)$$

where $P_1 \neq P_2$ are the interband momentum-matrix elements with the velocity dimension (we put $\hbar = 1$ in the intermediate formulas). Quadratic terms in the momentum \mathbf{k} can be written [16] in the main diagonal of the matrix (1), as well as in the terms, connecting the

states at the valence band top, $-\varepsilon_g$. We omit them, because their contribution in the DF is on the order of $1/\ln(\varepsilon_{at}/\varepsilon_g) \ll 1$, where ε_{at} is the energy of the atomic scale.

This Hamiltonian (1) gives rise to the eigenvalues

$$\varepsilon_{1,4} = \pm[\varepsilon_g^2 + P_1^2 k_z^2 + P_2^2 k_\perp^2]^{1/2}, \quad k_\perp^2 = k_x^2 + k_y^2, \quad (2)$$

corresponding with the conduction band and the light-hole band, and the twofold eigenvalue

$$\varepsilon_{2,3} = -\varepsilon_g, \quad (3)$$

for the heavy-hole band (see Fig. 1b).

The effective masses at the conduction-band bottom are

$$m_\parallel = \varepsilon_g/P_1^2, \quad m_\perp = \varepsilon_g/P_2^2 \quad (4)$$

for the longitudinal and transverse directions respectively to the main z -axis. Comparison with the values $m_\parallel = 0.065m_0$, $m_\perp = 0.068m_0$, and $2\varepsilon_g = 0.69$ eV obtained [8] in the experimental data analysis gives $P_1 = 0.966 \times 10^8$ cm/sec, $P_2 = 0.945 \times 10^8$ cm/sec.

The velocity operator has the form

$$\mathbf{v} = \frac{\partial H}{\partial \mathbf{k}} = \begin{pmatrix} 0 & iP_2\mathbf{e}_x & iP_2\mathbf{e}_y & iP_1\mathbf{e}_z \\ -iP_2\mathbf{e}_x & 0 & 0 & 0 \\ -iP_2\mathbf{e}_y & 0 & 0 & 0 \\ -iP_1\mathbf{e}_z & 0 & 0 & 0 \end{pmatrix}$$

with orthonormal vectors \mathbf{e}_j chosen along the coordinate axes.

Let us define the velocity matrix in the representation diagonalizing the Hamiltonian (1):

$$\tilde{\mathbf{v}} = U^\dagger \mathbf{v} U.$$

Using the eigenfunctions of the Hamiltonian, one finds the matrix U :

$$U = \begin{pmatrix} -a_1 & 0 & 0 & a_2 \\ ip_x/n_1 & -p_y/p_\perp & p_x p_z/p_\perp p & ip_x/n_2 \\ ip_y/n_1 & p_x/p_\perp & p_y p_z/p_\perp p & ip_y/n_2 \\ ip_z/n_1 & 0 & -p_\perp/p & ip_z/n_2 \end{pmatrix},$$

where we use the notations $p_z = P_1 k_z$, $p_{x,y} = P_2 k_{x,y}$, $p = \sqrt{p_z^2 + p_\perp^2}$, $n_{1,2} = \sqrt{2\varepsilon_1(\varepsilon_1 \pm \varepsilon_g)}$, $a_{1,2} = \sqrt{(\varepsilon_1 \pm \varepsilon_g)/2\varepsilon_1}$, and ε_1 is given in Eq. (2).

We note that the diagonal velocity-matrix elements in this representation coincide with the derivative of the eigenvalues

$$\langle i|\tilde{\mathbf{v}}|i\rangle = \frac{\partial \varepsilon_i}{\partial \mathbf{k}}$$

and we write the off-diagonal elements

$$\langle 1|\tilde{\mathbf{v}}|2\rangle = i\sqrt{\frac{\varepsilon_1 + \varepsilon_g}{2\varepsilon_1}} P_2 \frac{k_y \mathbf{e}_x - k_x \mathbf{e}_y}{k_\perp}, \quad (5)$$

$$\begin{aligned} \langle 1|\tilde{\mathbf{v}}|3\rangle &= \frac{-iP_1 P_2}{\sqrt{2\varepsilon_1(\varepsilon_1 - \varepsilon_g)}} \left[\frac{k_z}{k_\perp} (k_x \mathbf{e}_x + k_y \mathbf{e}_y) - k_\perp \mathbf{e}_z \right], \\ \langle 1|\tilde{\mathbf{v}}|4\rangle &= \frac{\varepsilon_g}{\varepsilon_1 \sqrt{\varepsilon_1^2 - \varepsilon_g^2}} (P_1^2 k_z \mathbf{e}_z + P_2^2 k_x \mathbf{e}_x + P_2^2 k_y \mathbf{e}_y), \\ \langle 3|\tilde{\mathbf{v}}|4\rangle &= \frac{-iP_1 P_2}{\sqrt{2\varepsilon_1(\varepsilon_1 + \varepsilon_g)}} \left[\frac{k_z}{k_\perp} (k_x \mathbf{e}_x + k_y \mathbf{e}_y) - k_\perp \mathbf{e}_z \right]. \end{aligned}$$

These matrix elements enter the general quantum-mechanic formula for the dynamic conductivity $\sigma_{\alpha\beta}(\omega)$ derived in the paper [13]. Then, we obtain the DF with the help of the relation

$$\epsilon_{\alpha\beta}(\omega) = 1 + 4\pi i \sigma_{\alpha\beta}(\omega)/\omega. \quad (6)$$

Due to the symmetry, the off-diagonal tensor components of the DF vanish and there are only two independent components $\epsilon_{zz}(\omega)$ and $\epsilon_{xx}(\omega) = \epsilon_{yy}(\omega)$.

The DF is separated into the intraband and interband parts. The intraband term contains only the diagonal velocity-matrix elements and has the Drude-Boltzmann form. For instance, we obtain for the degenerate electrons:

$$\epsilon_{zz}^{intra}(\omega) = -\frac{4e^2 P_1}{3\pi \hbar P_2^2} \frac{(\mu^2 - \varepsilon_g^2)^{3/2}}{\omega(\omega + i\nu)\mu}, \quad (7)$$

where the chemical potential μ , the relaxation rate ν and the photon frequency ω are written in the common units.

Neglecting the carrier relaxation, we can write the interband term for the extraordinary component of the DF in the form

$$\begin{aligned} \epsilon_{zz}^{inter}(\omega) &= 1 + \frac{2e^2}{\pi^2} \int d^3 k \left\{ \frac{[f(-\varepsilon_1) - f(\varepsilon_1)]|\tilde{v}_{14}^z|^2}{2\varepsilon_1[4\varepsilon_1^2 - (\omega + i\delta)^2]} \right. \\ &\quad + \frac{[f(-\varepsilon_g) - f(\varepsilon_1)]|\tilde{v}_{13}^z|^2}{(\varepsilon_1 + \varepsilon_g)[(\varepsilon_1 + \varepsilon_g)^2 - (\omega + i\delta)^2]} \\ &\quad \left. + \frac{[f(-\varepsilon_1) - f(-\varepsilon_g)]|\tilde{v}_{34}^z|^2}{(\varepsilon_1 - \varepsilon_g)[(\varepsilon_1 - \varepsilon_g)^2 - (\omega + i\delta)^2]} \right\}, \quad (8) \end{aligned}$$

where $f(\varepsilon) = 1/(\exp[(\varepsilon - \mu)/T] + 1)$ is the Fermi function. For the pristine semiconductor at low temperature, the conduction band is empty, but the chemical potential μ can be higher than the conduction band bottom ε_g in the case of doping (see Fig. 1b).

The different terms in the braces present the various optical transitions: first, between the light-hole band and the conduction band, second, between the heavy-hole band and the conduction band, and third, between the light- and heavy-hole bands. The infinitesimal δ in the denominators of Eq. (8) defines the bypass around the poles. These bypasses give the imaginary part of the DF, whereas the principal values of the integrals yield the real part.

Transforming the integration variables

$$k_x = \frac{\sqrt{\varepsilon_1^2 - \varepsilon_g^2}}{P_2} \sin \theta \cos \varphi, \quad k_y = \frac{\sqrt{\varepsilon_1^2 - \varepsilon_g^2}}{P_2} \sin \theta \sin \varphi,$$

$$k_z = \frac{\sqrt{\varepsilon_1^2 - \varepsilon_g^2}}{P_1} \cos \theta, \quad \frac{\partial(k_z, k_x, k_y)}{\partial(\varepsilon_1, \theta, \varphi)} = \frac{\varepsilon_1 \sqrt{\varepsilon_1^2 - \varepsilon_g^2}}{P_1 P_2^2} \sin \theta, \quad (9)$$

we integrate over the angles θ and φ :

$$\begin{aligned} \epsilon_{zz}^{inter}(\omega) = & \frac{8e^2 P_1}{3\pi \hbar P_2^2} \int_{\varepsilon_g}^{\varepsilon_{at}} d\varepsilon \sqrt{\varepsilon^2 - \varepsilon_g^2} \left\{ \frac{\varepsilon_g^2 [f(-\varepsilon) - f(\varepsilon)]}{2\varepsilon^2 [4\varepsilon^2 - (\omega + i\delta)^2]} \right. \\ & \left. + \frac{f(-\varepsilon_g) - f(\varepsilon)}{(\varepsilon + \varepsilon_g)^2 - (\omega + i\delta)^2} + \frac{f(-\varepsilon) - f(-\varepsilon_g)}{(\varepsilon - \varepsilon_g)^2 - (\omega + i\delta)^2} \right\} + 1. \end{aligned}$$

The integral presenting the real part of the DF diverges logarithmically at the upper limit. Since the leading contribution arises from the values $\varepsilon \sim (\mu, \omega)$, the integral can be cut off at the atomic value of energy ε_{at} , where our $\mathbf{k} \cdot \mathbf{p}$ expansion becomes incorrect. The imaginary part is easily evaluated for zero temperatures. For instance, we find for the case $\mu > \varepsilon_g$, when electrons fill the conduction band,

$$\begin{aligned} \text{Im } \epsilon_{zz}^{inter}(\omega) = & \frac{4e^2 P_1}{3\hbar P_2^2} \left\{ \frac{\varepsilon_g^2}{2\omega^2} \sqrt{1 - \frac{(2\varepsilon_g)^2}{\omega^2}} \theta(\omega - 2\mu) \right. \\ & \left. + \sqrt{1 - \frac{2\varepsilon_g}{\omega}} \theta(\omega - \varepsilon_g - \mu) \right\}, \quad (10) \end{aligned}$$

where the step θ -function conveys the condition for the interband electron absorption.

Let us emphasize, that the band edge for the optical transitions into the conduction band from the light-hole band at $\omega = 2\mu$ is higher than the edge for the transition from the heavy-hole band at $\omega = \varepsilon_g + \mu$. With increasing the free electron concentration, both edges demonstrate the blue Burstein-Moss shift. At zero temperatures, the chemical potential μ , measured from the midgap is determined by the free-electron concentration: $n_0 = (\mu^2 - \varepsilon_g^2)^{3/2} / 3\pi^2 \hbar^3 P_1 P_2^2$.

If the electrons are absent in the conduction band, $-\varepsilon_g < \mu < \varepsilon_g$, the imaginary part of the DF is given in Eq. (10) with substitution $\mu \rightarrow \varepsilon_g$. Far away from the absorption edges, where $\omega \gg \varepsilon_g + \mu$, the imaginary part demonstrates the plateau-like character with

$$\max \text{Im } \epsilon^{inter}(\omega) = \frac{4e^2 P_1}{3\hbar P_2^2}. \quad (11)$$

The plateau noticed also in the paper [12] and for the A_4B_6 semiconductors in [14] is a consequence of the linearity of the electron dispersion at the energy larger in comparison with the energy gap.

The real part of the DF contains the following contributions. The transitions between the heavy-hole bands and the conduction band give

$$\begin{aligned} \text{Re } \epsilon_{zz}^{c, hh}(\omega) = & \frac{8e^2 P_1}{3\pi \hbar P_2^2} \left\{ \ln \frac{2\varepsilon_{at}}{\mu + \sqrt{\mu^2 - \varepsilon_g^2}} + \frac{\sqrt{1+2x}}{2} \right. \\ & \left. \times \ln \frac{\mu + (\mu + \varepsilon_g)x + \sqrt{(\mu^2 - \varepsilon_g^2)(1+2x)}}{(\mu + \varepsilon_g + \omega)(1+x + \sqrt{1+2x})} + F(x) \right\} \quad (12) \end{aligned}$$

where

$$F(x) = \frac{\sqrt{1-2x}}{2} \ln \frac{\mu - (\mu + \varepsilon_g)x + \sqrt{(\mu^2 - \varepsilon_g^2)(1-2x)}}{|\omega - \mu - \varepsilon_g|(1-x + \sqrt{1-2x})}, \quad (13)$$

if $x = \varepsilon_g/\omega < 1/2$ and

$$F(x) = -\sqrt{2x-1} \arctan \frac{\omega \sqrt{2x-1}}{\mu + \varepsilon_g - \omega + \sqrt{\mu^2 - \varepsilon_g^2}},$$

if $x > 1/2$.

The transitions between the light-hole band and the conduction band contribute

$$\begin{aligned} \text{Re } \epsilon_{zz}^{c, lh}(\omega) = & \frac{4e^2 P_1 x^2}{3\pi \hbar P_2^2} \left\{ 1 - \sqrt{1 - \varepsilon_g^2/\mu^2} \right. \\ & \left. + \sqrt{1 - 4x^2} \ln \frac{\sqrt{\mu^2 - \varepsilon_g^2} + \mu \sqrt{1 - 4x^2}}{|(\omega/2)^2 - \mu^2|^{1/2} (1 + \sqrt{1 - 4x^2})} \right\} \quad (14) \end{aligned}$$

for $x < 1/2$ and

$$\begin{aligned} \text{Re } \epsilon_{zz}^{c, lh}(\omega) = & \frac{4e^2 P_1 x^2}{3\pi \hbar P_2^2} \left\{ 1 - \sqrt{1 - \varepsilon_g^2/\mu^2} \right. \\ & \left. - \sqrt{4x^2 - 1} \arctan \frac{(1 - \sqrt{1 - \varepsilon_g^2/\mu^2}) \sqrt{4x^2 - 1}}{\sqrt{1 - \varepsilon_g^2/\mu^2} - 1 + 4x^2} \right\} \quad (15) \end{aligned}$$

for $x > 1/2$.

We find that the real part of the DF as a function of ω takes at $x = 1/2$ the maximal value for $\mu = \varepsilon_g$:

$$\begin{aligned} \max \text{Re } \epsilon_{zz}^{inter} = & 1 + \frac{8e^2 P_1}{3\pi \hbar P_2^2} \\ & \times \left[\ln \frac{2\varepsilon_{at}}{\varepsilon_g} - \frac{\ln(3+2\sqrt{2})}{\sqrt{2}} + \frac{1}{8} \right]. \quad (16) \end{aligned}$$

If the carriers appear in the conduction band, $\mu > \varepsilon_g$, the real part of the DF has a logarithmic singularity smeared with temperature or carrier relaxation. For small relaxation rate ν in comparison with the photon frequency ω , we have in Eqs. (10), (13), (14) to substitute

$$\begin{aligned} \theta(\omega - \omega_{at}) & \rightarrow \frac{1}{2} + \frac{1}{\pi} \arctan[(\omega - \omega_{at})/2\nu] \quad (17) \\ (\omega - \omega_{at})^2 & \rightarrow (\omega - \omega_{at})^2 + (2\nu)^2, \end{aligned}$$

where ω_{at} is the absorption edge equal to $\varepsilon_g + \mu$ or 2μ for the corresponding transitions. If temperature plays a more important role, we should put T instead of ν in Eq. (17).

So far the extraordinary component ϵ_{zz} was presented. The ordinary component ϵ_{xx} differs only in the factor P_2/P_1 , which equals 0.98 for the experimental values of the effective masses (4).

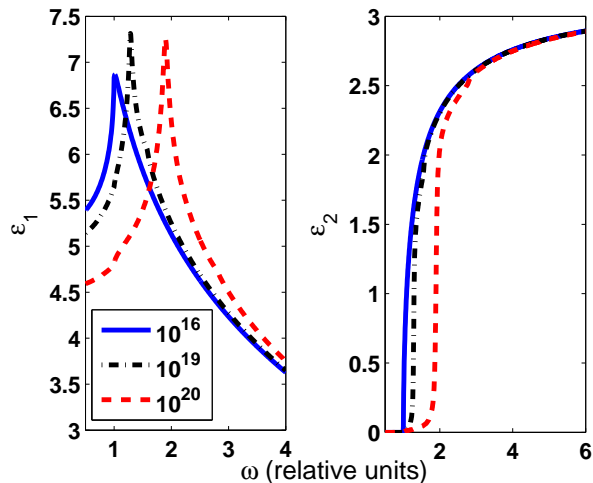


FIG. 2: The real and imaginary parts of the DF versus the photon frequency (in units of the gap $2\varepsilon_g = 0.69$ eV) for various free-electron concentrations, corresponding values of the chemical potential μ are 1.01, 1.57, 2.79 (in units of $2\varepsilon_g = 0.69$ eV); relaxation rate $\nu = 0,01 \mu$.

Now the value of the cutoff parameter ε_{at} is only needed to calculate the DF. To estimate this value, we can use the energy arising in the Kane model while the quadratic terms are taken into account. According to estimations [8, 12], this energy ranges from 8 to 15 eV. We take the intermediate value $\varepsilon_{at} = 10$ eV plotting Fig. 2, where our theoretical results are shown. The maximum value of the real part, Eq. (16), is found to equal 6.91 and the imaginary part of the DF takes the value

3.16 on the plateau, Eq. (11). The corresponding values, $2.5 \div 3.5$, obtained from experiments [17, 18, 19] and calculated from the first principles [12] are on the plateau in the frequency range $1.5 \div 4.0$ eV. That agrees very well with Fig. 2 (right panel). The experiment [18] finds the value about $\simeq 9$ for the maximum of the real part. The estimation [18] of the dielectric constant gives $\varepsilon_\infty = 6.7$. The *ab initio* calculations [12, 20] find correspondingly in these two papers $\varepsilon_\infty(xx) = 7.03$ and 7.16 , as well as $\varepsilon_\infty(zz) = 7.41$ and 7.27 . The agreement with our Fig. 2 (left panel) is excellent again. In our calculations, the maximum of the real part for the large carrier concentration increases logarithmically with decreasing of the relaxation rate. Plotting Fig. 2, we take $\nu = 0.01\mu$ for various carrier concentrations.

Concerning the dielectric constant ε_∞ , we keep in mind that the phonons contribute to its value. This contribution can be estimated as ω_{TO}^2/ω^2 , where ω_{TO} is the transverse phonon frequency which is much less than the photon frequency considered here. Therefore, the phonon contribution into ε_∞ should be considered as negligible.

In conclusions, we find analytically that the real part of the DF contains a singular contribution from the interband optical transitions. It presents the large logarithmic term to the optical dielectric constant. While increasing the frequency, we obtain the dispersion of the dielectric function. Near the edge of the interband absorption, a peak appears in the real part of the DF for degenerate electrons filled the conduction band if the relaxation rate is large enough.

This work was supported by the Russian Foundation for Basic Research (grant No. 07-02-00571). The author is grateful to the Max Planck Institute for the Physics of Complex Systems for hospitality in Dresden.

-
- [1] V. Y. Davydov et al., Phys. Status Solidi B **229**, R1 (2002).
- [2] J. Wu, W. Walukiewicz, K.M. Yu et al., Appl. Phys. Lett. B **80**, 3967 (2002).
- [3] Y. Nanishi, Y. Saito, and T. Yamaguchi, Jpn. Appl. Phys., Part 1 **42**, 2549 (2003).
- [4] A. Sher, M. van Schilfgaarde, M.A. Berding et al., MRS Internet J. Nitride Semicond. Res. **4S1**, G5.1 (1999).
- [5] F. Bechstedt and J. Furthmüller, J. Cryst. Growth **246**, 315 (2002).
- [6] J. Wu, W. Walukiewicz, W. Shan et al., Phys. Rev. B **66**, 201403 (2002).
- [7] S.P. Fu, Y.F. Chen, Appl. Phys. Lett. **85**, 1523 (2004).
- [8] Patric Rinke, M. Winkelnkemper, A. Qteish et al., Phys. Rev. B **77**, 075202 (2008).
- [9] D. Bagayoko, L. Franklin, H. Jin, and G.L. Zhao, Phys. Rev. B **76**, 037101 (2007).
- [10] E.O. Kane, J. Phys. Chem. Solids **1**, 249 (1957); E.O. Kane, in *Band Theory and Transport Properties, Handbook on Semiconductors*, vol. 1, ed. by W. Paul (North-Holland, Amsterdam, 1982) p. 195.
- [11] R. Goldhahn, P. Schley, A.T. Winzer et al., J. Cryst. Growth **288**, 273 (2006).
- [12] J. Furthmüller, P.H. Hahn, F. Fuchs, and F. Bechstedt, Phys. Rev. B **72**, 205106 (2005).
- [13] L.A. Falkovsky, A.A. Varlamov, Eur. Phys. J. B **56**, 281 (2006); L.A. Falkovsky, S.S. Pershoguba, Phys. Rev. B **76**, 153410 (2007).
- [14] L.A. Falkovsky, Phys. Rev. B **77**, 193201 (2008).
- [15] J.S. Thakur, Y.V. Danylyuk, D. Haddat et al., Phys. Rev. B **76**, 035309 (2007).
- [16] S.L. Chuang and C.S. Chang, Phys. Rev. B **54**, 2491 (1996).
- [17] R. Goldhahn, S. Shokovets, V. Cimalla et al., Mater. Res. Soc. Symp. Proc. **743**, L5.9 (2003).
- [18] A. Kasic, E. Valcheva, B. Monemar et al., Phys. Rev. B **70**, 115217 (2004).
- [19] R. Goldhahn, A.T. Winzer, V. Cimalla et al., Superlattices Microstruct. **36**, 591 (2004).
- [20] N.E. Christensen and I. Gorczyca, Phys. Rev. B **50**, 4397 (1994).